Chalcogenide Letters Vol. 16, No. 11, November 2019, p. 545 - 555

DENSE CHALCOPYRITE $CuInSe_2$ THIN FILMS PREPARED WITH ETHANOL-BASED In_2Se_3-Cu^+ INK

X. HUANG[a], X. L. CHEN[b], Z. W. ZHENG[a], H. M. JI[a,*], Y. L. MA[b]
[a]*Key Laboratory of Advanced Ceramics and Machining Technology of Ministry of Education, School of Materials Science and Engineering, Tianjin University, Tianjin 300072, China*
[b]*College of Physics and Electronic Information Engineering, Qinghai University for Nationalities, Xining 810007, China*

Here, we show a novel ink containing ethanol, In_2Se_3 nanosheets and Cu^+ that can be used as the sol for filming by dip coating method. And pure chalcopyrite (CH) $CuInSe_2$ (CIS) thin films were obtained when In_2Se_3 nanosheets with poor crystallinity as a component of the ink. We described the formation of the CH CIS films that exhibit (112)-orientation and dense structure without interspace. Hall measurement shows that the CIS film sintered at 550 ºC has an electrical resistivity of 3.19 Ω·cm and carrier concentration of 2.63×10^{17} cm^{-3}, which meet the requirements of high performance solar cell absorption layer.

(Received July 24, 2019; Accepted November 18, 2019)

Keywords: $CuInSe_2$, In_2Se_3 nanosheets, Hot injection, Ink, Thin film

1. Introduction

With the continuous reduction of non-renewable energy sources and people's increasing awareness of environmental protection, the rapid development of solar cell makes it particularly eye-catching. CIS-based compounds ($CuInSe_2$, $CuIn_xGa_{1-x}Se_2$, $CuInS_xSe_{2-x}$, ect.) have been used as high-performance solar cell absorbing layers due to their adjustable direct bandgap (1.0-2.4 eV) and high visible absorption coefficient (>10^5 cm^{-1}) [1]. So far the highest conversion efficiency of polycrystalline thin film solar cells is 22.9 % measured for a 1-cm^2 $CuIn_xGa_{1-x}Se_2$ solar cell [2]. High performance CIS solar cells require a dense absorber of carefully controlled stoichiometry, which mainly obtained by expensive multistep vacuum-based techniques [3,4]. In an effort to reduce fabrication costs relative to vacuum-based approaches and produce large area thin films with wide application, solution-deposition thin film based on non-vacuum technology has been pursued. CIS-based compounds nanoparticles synthesized by liquid phase method are dispersed in organic solution to obtain nanoink. Then the ink is deposited on the substrates for heat treatment [5-7]. Despite the high utilization of raw materials and low cost, the nanoparticles with high crystallinity and melting point will not grow significantly during heat treatment, and the volatilization of macromolecular solvents will destroy the densification of films. Compared with the above method, it is noted that high quality films are often obtained by heat treatment of precursor layers prepared by directly dissolving Cu-Se, In-Se, Ga-Se or metal salts in solvents [8-11]. The reason is that $CuSe_x$ (x=1, 2) is peritectic decomposed into liquid phase which can

*Corresponding author: jihuiming@tju.edu.cn

promote crystal growth and densification during sintering [12,13]. However, in their studies, highly toxic H_2S or H_2Se gas are introduced to grow the grains [8] or more dangerous hydrazine is used as solvent to dissolve bulk raw materials [9-11], which are not conducive to production safety. The challenges must still be addressed.

Here, we present a facile, clean and low-cost solution method to deposit high-quality CIS films. Given that the CuCl is insoluble in ethanol, the 2-amino-2-methyl-1-propanol (AMP) was added to ethanol to dissolve CuCl by forming Cu-amino complex. The prepared In_2Se_3 nanosheets, easily dispersed in ethanol, were mixed with Cu-amino complex to obtain hybrid ink, which was deposited on glass by dip coating and annealed in Se vapor. This process not only avoids the use of dangerous solvents to dissolve Cu-Se or In-Se, but also creates conditions for the formation of CuSe. Moreover, no amorphous nanosheets have been reported as precursor layers before. We obtained (112)-oriented dense CIS films using amorphous In_2Se_3 nanosheets. And the formation of (112)-orientation is accompanied by surface reconstruction, which will reduce the open circuit voltage loss caused by recombination loss through dangling bonds at the GBs [14,15].

2. Experimental

2.1. Chemicals

Selenium powder (Se, 99.9%), copper(I) chloride (CuCl 97%), indium(III) chloride ($InCl_3$•$4H_2O$, 99.9%), polyvinylpyrrolidone (PVP, Mw = 58000) and hydrazine hydrate (N_2H_4·H_2O, 98%) were purchased from Aladdin and directly used as received without further processing. 2-amino-2-methyl-1-propanol (Yuanye Bio-Technology, AMP, 93~97%), absolute ethanol (Hengshan chemicals, CH_3CH_2OH, 99.7%) and triethylene glycol (Aladdin, TEG, 98%) were used as solvents.

2.2. Synthesis of In_2Se_3 nanoink

The familiar hot-injection process was used to fabricate In_2Se_3. Firstly, 0.4 mmol of the $InCl_3$•$4H_2O$ (0.1173 g) was dissolved thoroughly in 10 mL of the TEG in a beaker so as to the indium precursor solution was obtained. Then a three-necked flask containing 0.6 mmol of Se (0.0474 g), 0.06 g PVP, and 40 mL TEG was assembled into a hot reflux device with nitrogen stream. Subsequently, 0.1 mL N_2H_4·H_2O was injected into the three-necked flask. The solution in flask was then heated to 250 ºC or 270 ºC under magnetic stirring, which followed by drop-by-drop injection of the as-prepared indium precursor solution at a rate of 1 ml/min. The solution was rapidly cooled after refluxing for 30 minutes at the corresponding injection temperature. Finally, the solution was centrifuged and washed several times with anhydrous ethanol, and then the obtained In_2Se_3 was dispersed in 6 mL ethanol for reserve.

2.3. Preparation of In_2Se_3-Cu^+ ink

3 mmol of CuCl (0.2970 g) was dissolved in a mixed solution of 1 mL of AMP and 5 mL of ethanol to obtain a 0.5 mol/L Cu^+ solution. The Cu^+ solution was added to the In_2Se_3 ink according to the ratios shown in Table 1, leading to two sorts of hybrid ink after half an hour of ultrasound dispersion. The reason for selecting these two ratios is that the atomic contents of copper and indium in the precursor layer obtained by ink deposition are substantially the same.

Table 1. The composition of two sorts of In_2Se_3-Cu^+ ink.

Sample number	1#	2#
Synthesis temperature of In_2Se_3	250 ºC	270 ºC
n_{Cu} : n_{In}	1 : 2	1 : 1

2.4. Deposition and sintering of CIS precursor films

The CIS precursor films were fabricated by depositing the two kinds of ink on the glass slides layer by layer using the dip coater. (Before that the slides were ultrasonic cleaned with hydrochloric acid, acetone, deionized water and absolute ethanol successively.) The films were then placed in a graphite crucible containing selenium powder, followed by a heat treatment at 550 ºC for an hour in the argon-filled tube furnace. Having identified the denser CIS films originating from 1# ink, we turned our attention to the formation of dense films. So the coated substrates with 1# ink were annealed at 300 ºC, 400 ºC, 500 ºC and 600 ºC for 30 min. The process flow chart is shown in Fig. 1 (taking the synthesis of 1# ink as an example).

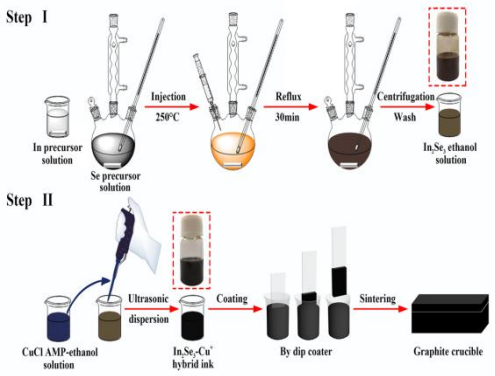

Fig. 1. Flow chart of preparation, deposition and sintering of 1# ink.

2.5. Materials characterization

The XRD date were obtained with X-ray powder diffractometer (XRD, Bruker D8 Advanced, Germany) with Cu *K*α radiation at 40 kV and 40 mA. The microstructures and element content of the products were characterized using scanning electron microscope (SEM, JSM 7800F, Japan), transmission electron microscopy (TEM, JEM 2100F, Japan) and their respective energy dispersive spectroscopy. The bonding states of the synthesized products were analyzed by Raman spectrometer (Renishaw inVia reflex, England) with 532 nm laser wavelength. Hall measurement was detected by physical property measurement system (PPMS, Quantum Design PPMS-9, America).

3. Result and discussion

3.1. Characterization of In_2Se_3 nanosheets

Powder X-ray diffraction (PXRD) patterns are displayed in Fig. 2a, b for In_2Se_3 powder samples synthesized at 250 ºC and 270 ºC. It shows that single trigonal β-In_2Se_3 (JCPDS file 35-1056) with good crystallinity was formed at 270 ºC, while nearly amorphous In_2Se_3 at 250 ºC. Although the In_2Se_3 of Fig. 2a is poor in crystallinity, most of the diffraction peaks can be indexed to hexagonal β-In_2Se_3 (JCPDS file 40-1048).

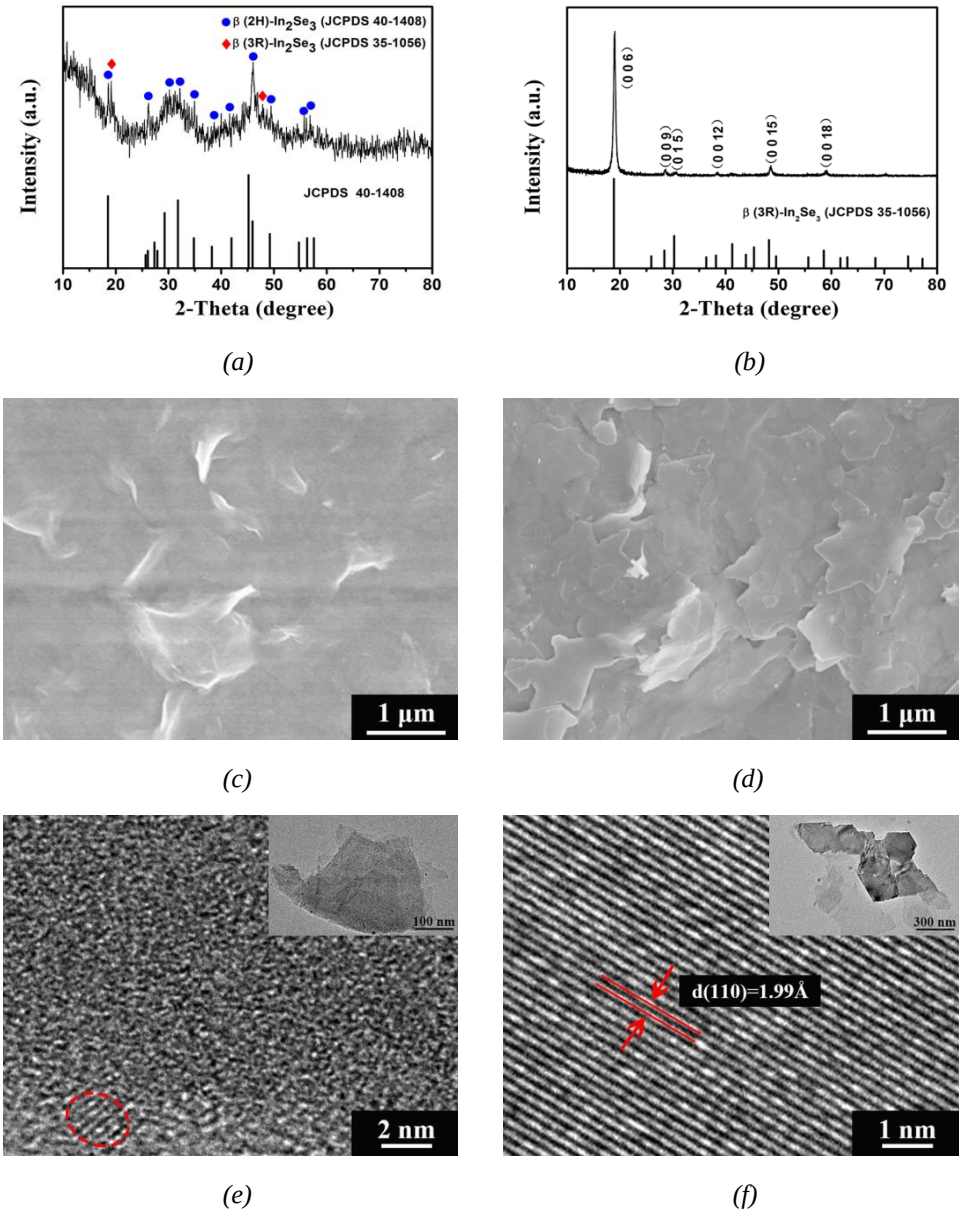

Fig. 2. PXRD diffractograms, SEM images and HRTEM images of In_2Se_3 were obtained by reaction at 250 ºC (a, c, e) and 270 ºC (b, d, f), respectively. Insets are corresponding TEM images.

Fig. 2c, d give the SEM images of the In_2Se_3 dried after being dispersed in ethanol. The sharp nanosheets with average diameter being around 1 μm can be observed at 270 ºC (Fig. 2d).

However, as we depicted in Fig. 2c, the amorphous In_2Se_3 nanosheets are tiled on the substrate and no particle edges are observed. It can be inferred that $InSe_4$ molecular units in amorphous In_2Se_3 are strongly linked with each other [16], which assembles the nanosheets into films.

The transmission electron microscope (TEM) images of the In_2Se_3 synthesized at 250 °C and 270 °C (illustrations in Fig. 2e, f) show In_2Se_3 are formed by stacking ultra-thin nanosheets. Fig. 2e is high resolution transmission electron microscope (HRTEM) image of the product obtained at 250 ºC, showing that only the elliptically labeled lattice fringes with a diameter of about 2 nm are found, which is consistent with the poor crystallinity exhibited by Fig. 2a. And Fig. 2f indicates the distances between the adjacent lattice fringes to be 1.99 Å, which corresponds with the (110) d-spacing for trigonal β-In_2Se_3, and agrees well with the XRD result (Fig. 2b). Taken together, these results demonstrate a higher temperature is favorable for crystallization, and In_2Se_3 with poor crystallinity can easily lay into a dense structure.

3.2. Characterization of CIS absorber layer

Films deposited with precursor inks labeled 1# and 2# were selenized and sintered at 550 ºC. Fig. 3a shows that both films have strong (112)-orientation, especially the film selenized from 1# ink has only one strong diffraction peak at 26.4º indexed to CH CIS (JCPDS file 40-1087). The peak at about 30.5º corresponds to γ-In_2Se_3 in 2#, and the (112) diffraction peak is extremely asymmetric and can be divided into peaks of CIS and ordered defect compound (ODC). The cation vacancies in the ODC reduce the effective cation radius [17], and the unit cell size decreases according to Vegard's law, so that the diffraction peak shifts to the right. The Raman spectra displayed in Fig. 3b shows a prominent peak at 174 cm^{-1} corresponding to A_1 mode of CIS [18] and no A_1 mode at 260 cm^{-1} of Cu-Se [19,20] in 1#, which further support that the film sintered from 1# ink is free of secondary phases. Besides the A_1 mode at 174 cm^{-1}, Raman spectra of the 2# exhibits A_1 mode at 153 cm^{-1} results from the motion of the Se atom of ODC [21,22] and the broadened peak of 228 cm^{-1} mode related to the γ-phase of In_2Se_3 [23], which is consistent with the results in Fig. 3a.

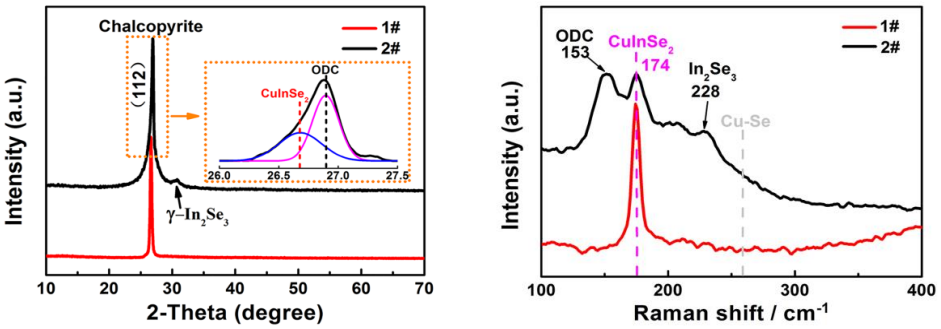

Fig. 3. XRD patterns (a) and Raman spectra (b) of thin films annealed at 550 ºC for 60 min. 1# and 2# in the legends represent sintered films deposited with 1# ink and 2# ink respectively.

As shown in Fig. 4a, c, the surface of the film prepared by 1# ink is smooth before heat treatment but rough after heat treatment. After annealing, no pores are observed on the surface and inside of the film and the film thickness is reduced by approximately 47.6%, indicating that the film structure is dense, which is beneficial to electron transport.

It can be clearly seen in Fig. 4b that the film prepared by 2# ink is stacked by a number of layers of In_2Se_3 nanosheets. And Copper ions should be on the surface of nanosheets. In sharp contrast to Fig. 4c, the sintered film deposited from 2# ink is loose and multi-layered, with obvious cracks between layers (inset of Fig. 4d). Furthermore, the local magnification in Fig. 4d shows that the surface of the film is still composed of well-defined nanosheets, on which a large number of particles of tens of nm are grown. In addition, the morphology and size of the product are similar to those of the In_2Se_3 nanosheets in the precursor layer. And high diffusivity of copper was demonstrated by Krishnan and Wood [13]. It becomes clear that the formation of ODC and CIS mainly depended on solid state reaction and the formation kinetics were dominated by the diffusion of copper ions. Given that the film was sintered in Se vapor, Cu-Se compounds might be formed on the surface of nanosheets. The diffusion of copper ions into In_2Se_3 nanosheets resulted in the formation of ODC. And copper vacancy sites, which are abundant in ODC, can play a significant role in the migration of indium ions [24,25]. Then indium ions moved to the interface between ODC and Cu-Se compounds following the path of copper vacancy sites, and reacted with Cu-Se compounds to form CIS.

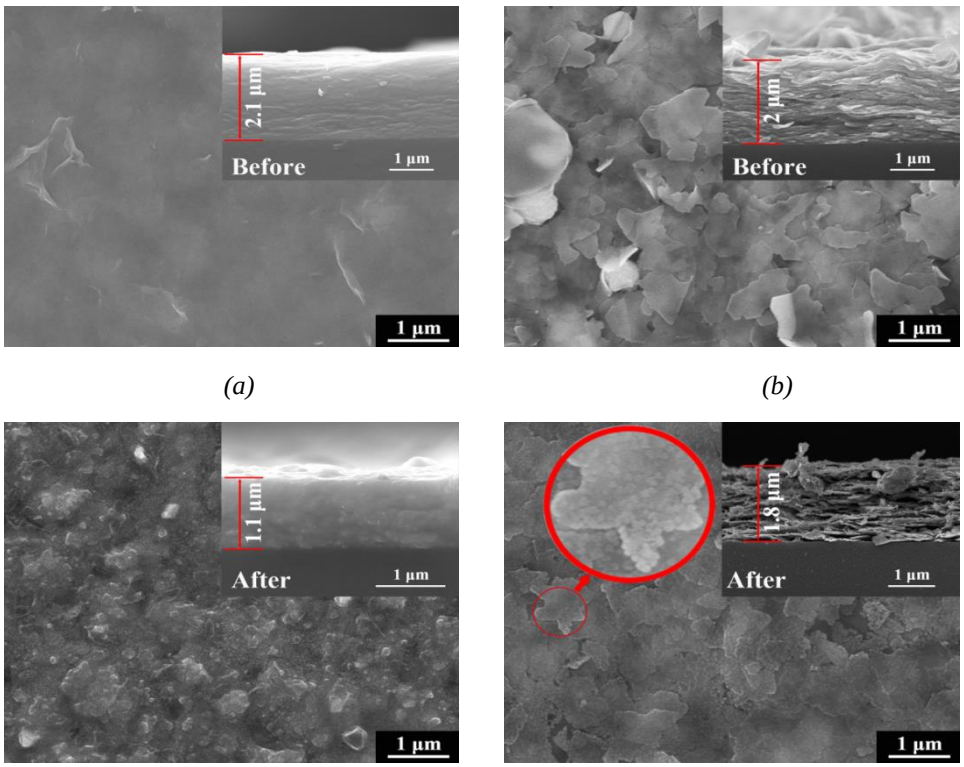

Fig. 4. Surface and cross-sectional SEM images of films deposited with precursor inks labeled 1# (a, c) and 2# (b, d) before and after annealing at 550 ºC for 60 min.

3.3. Formation of dense CIS thin film

In view of the denser structure and single CH phase of the film made from 1# ink, We heat treated the films deposited by 1# ink at 300 ºC, 400 ºC, 500 ºC and 600 ºC. As shown in Fig. 5, after annealing at 300 °C or higher, the crystal growth of the film maintains a distinct orientation. And the full width at half maximum (FWHM) of the peak near 2θ=26.6º decreases with increasing temperature, indicating that the film crystallinity is improved. Furthermore, consistent with the results in Fig. 3a, (112)-oriented α-CIS was obtained at temperatures above 500 ºC. It is reasonable that the surface energy of (112) surface in CH structure is the lowest, and for the (112) surface, (Cu, In)-vacancy pair, V_{Cu} and Cu_{In} have lower energies [26].

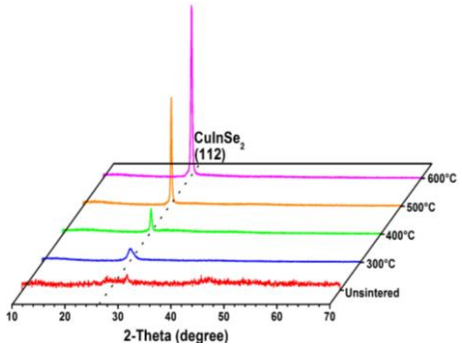

Fig. 5. XRD patterns of pre-formed thin films prepared by dip coating of 1# ink before and after annealing in a Se/Ar atmosphere at 300 ºC, 400 ºC, 500 ºC and 600 ºC.

Furthermore, we collected the corresponding XRD data of the unannealed films (Fig. 6a) that showed characteristic peaks of β-In_2Se_3 (JCPDS file 40-1048), sphalerite CIS (JCPDS file 70-3084) and Cu_2Se (JCPDS file 04-0839), indicating that In_2Se_3 reacted with Cu^+. As we know, In_2Se_3 is stable by weak van der Waals force between layers which leaves one-third of possible indium sites empty [27,28]. The formation of CIS results from the substitution of Cu cations for indium cations and the direct occupancy of indium vacancies in In_2Se_3 lattices by Cu ions [29]. However, to the best of our knowledge, the formation of Cu_2Se from In_2Se_3 and Cu^+ at room temperature has not been reported before. This is related to the instability of amorphous In_2Se_3 nanosheets. When Cu^+ cations were added, the Se^{2-} in amorphous In_2Se_3 combined with Cu^+ cations to form more stable Cu_2Se. The reaction equations can be described as follows:

$$3Cu^+ + 2In_2Se_3 \rightarrow 3CuInSe_2 + In^{3+} \quad (1)$$

$$6Cu^+ + In_2Se_3 \rightarrow 3Cu_2Se + 2In^{3+} \quad (2)$$

This caused the ink to change from brown to black at the moment of mixing and the indium content in the nanosheets decreased while the Cu content increased. Therefore, a small amount of Cu cations were added to the amorphous In_2Se_3 while the content of Cu and indium in the precursor layer is the same.

The XRD peaks near 2θ=26.6º of the films annealed at 300 ºC and 400 ºC are shown in the illustration in Fig. 6a. The peaks are all superimposed by multiple peaks. However, the diverse

structure of Cu_xSe and CIS leads to XRD peaks close to each other and even coincide. It is difficult to decide the specific composition corresponding to the peaks. Raman spectroscopy can be used as a complementary means of XRD to characterize the binary and ternary phases that may exist. Fig. 6b is Raman spectra corresponding to the films in Fig. 5 to demonstrate and complement the previous results regarding the composition of films. The peaks of CH CIS are detected at 174 cm^{-1} (A_1 vibrational mode), 213 cm^{-1} (B_2,E mode) and 231 cm^{-1} (B_2,E mode) [18,30,31] in the thin films annealed at 500 ºC and 600 ºC. And no secondary phase is found. The other films have peaks at 258-262cm^{-1} related to Cu-Se binary compounds [19,20,32]. In addition, sphalerite (S) CIS [33] and Cu-Au (CA) order metastable CIS [34] may exist, which causes the peak at 174 cm^{-1} to shift right to 180 cm^{-1}. Sphalerite CIS precipitates in Cu_2Se, which also belongs to the face-centered cubic lattice. Because indium can rapidly diffuse by means of copper vacancies in Cu_2Se [24]. Sphalerite CIS is unstable at temperatures above 340 ºC and will transform into CH structure [33], while the difference of the peaks at 180 cm^{-1} is not significant in the Raman spectra of films annealed at 300 ºC and 400 ºC, indicating that the CA ordered structure is the main reason for the peaks at 180 cm^{-1}. B. Barcones [34] reported both domains form a (112) CH ∥ (011) CA interface between CA and CH domains. Therefore, we speculate that the formation of the (112) oriented CH thin films may be related to the long-term existence of CA structure. Or the (112) oriented films creates conditions for the existence of CA structure. With the increase of temperature, metastable CA order CIS finally transforms into CH CIS (Fig. 6b).

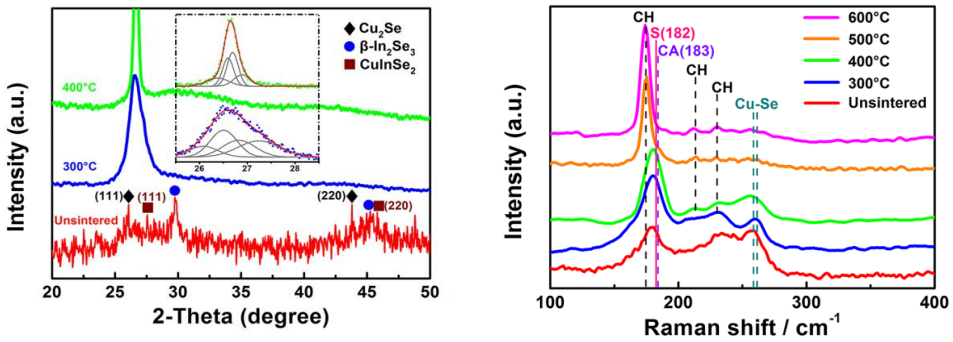

(a) *(b)*

Fig. 6. XRD patterns (a) and Raman spectra (b) of pre-formed thin films prepared by dip coating of 1# ink before and after annealing in a Se/Ar atmosphere at different temperatures.

Moreover, these Raman spectra provide direct evidence that Cu-Se compounds exist in the early stage of sintering, which is critical to forming a dense high-quality film. Initially, Cu_2Se was found in the unannealed films (Fig. 6a). And the following reactions occurs when Cu_2Se is heat-treated under a Se atmosphere [12,35,36]:

$$Cu_2Se + Se_{(vapor)} \rightarrow 2CuSe \quad (3)$$

$$T = 382\ ^{\circ}C \qquad (2-x)CuSe \rightarrow Cu_{2-x}Se + (1-x)Se_{(liquid)} \quad (4)$$

Before 382 ºC, the formation of CIS depends on solid state reaction. Heterogeneous nucleation at the initial interface will make the reaction saturated rapidly, and subsequent growth of CIS comes from ion diffusion. However, thickening of products will act as a diffusion barrier [37]. Upon heating to 382 °C, the peritectic decomposition of CuSe can provide liquid phase to promote ion diffusion and densification sintering. We illustrate this point in Fig. 7, which shows the cross-sectional morphology of the films. The thickness of the film after annealing at 400 °C is reduced sharply by 0.55 μm compared to 300 °C annealing, resulting from the influence of liquid phase sintering. That being said, liquid Se promotes flow and mass transfer and reduces micropores in thin films. In addition, the dense structure is always exhibited in Fig. 7, which facilitates ion diffusion during sintering to obtain a single CIS film.

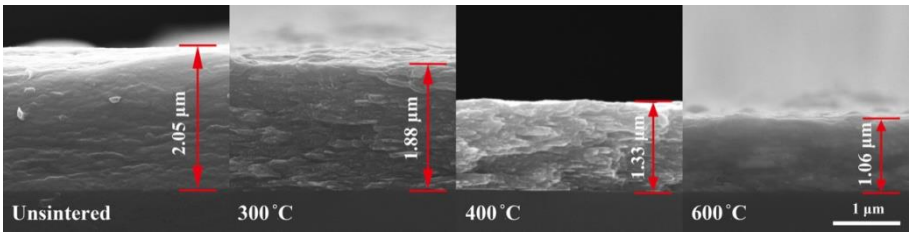

Fig. 7. Cross-sectional SEM images of pre-formed thin film prepared by dip coating of 1# ink before and after annealing in a Se/Ar atmosphere at 300 ºC, 400 ºC and 600 ºC.

Given that the film exhibited the potential characteristics of a high-quality absorbor, we tested its electrical properties (Table 2). The Hall measurement shows that the annealed film has characteristics of p-type semiconductor, and the electrical resistivity, carrier concentration and mobility are 3.19 Ω·cm, 2.63×10^{17} cm^{-3} and 7.43 cm^2 V^{-1} S^{-1}, respectively. From the above, The CIS film not only exhibits compact structure and single component, but also satisfies the optimum range of carrier concentration in high-efficiency devices [38].

Table 2. Electrical resistivity, carrier concentration and mobility of the film prepared by dip coating of 1# ink after annealing at 550 ºC.

	Electrical resistivity/ Ω·cm	Carrier concentration/ cm^{-3}	Carrier mobility/ cm^2 V^{-1} S^{-1}
CIS	3.19	2.63×10^{17}	7.43

4. Conclusions

In this paper, we have described the synthesis of chalcopyrite $CuInSe_2$ thin films with pure-phase and dense-structure by solution method using a novel ethanol-based In_2Se_3-Cu^+ ink. And some conclusions can be draw as follows. The morphology and composition of the films were strongly dependent on the crystallinity of In_2Se_3, which is related to reflux temperature. The high-quality films were obtained as a result of the tight combination of amorphous In_2Se_3

nanosheets in the precursor layer and the formation of liquid Se during sintering to promote ion diffusion and film densification. The thin films have excellent electrical properties to meet the requirements of absorption layer for high performance solar cells. Besides, the preparation process is simple, low cost and environmentally friendly. Non-toxic ethanol is used as a solvent for the ink, which can be mass-produced. Most importantly, the use of amorphous nanosheets provides a new way of thinking about the preparation of related materials.

Acknowledgements

The authors acknowledge the financial support from Key Natural Science Foundation of Qinghai province (2017-zj-729).

References

[1] M. Venkatachalam, M.D. Kannan, N. Muthukumarasamy, S. Prasanna, S. Jayakumar, R. Balasundaraprabhu, M. Saroja, Sol. Energy **83**(9), 1652 (2009).
[2] T. Kato, J. Wu, Y. Hirai, H. Sugimoto, V. Bermudez, IEEE J. Photovolt. **9**(1), 325 (2019).
[3] J. Posada, M. Jubault, A. Bousquet, E. Tomasella, D. Lincot, Prog. Photovolt: Res. Appl. **26**(1), 24 (2018).
[4] M. A. Contreras, K. Ramanathan, J. Abushama, F. Hasoon, D.L. Young, B. Egaas, R. N. Noufi, Prog. Photovolt: Res. Appl. **13**(3), 209 (2010).
[5] H. Liu, Z. Jin, W. Wang, Y. Wang, H. Du, Mater. Lett. **81**, 173 (2012).
[6] Y. Qi, Q. Hao, G. Ren, C. Liu, H. Liu, Ferroelectrics **521**(1), 132 (2017).
[7] Y. C. Chen, Y. P. Lin, T. E. Hsieh, M. W. Huang, J. Alloy. Compd. **791**, 1 (2019).
[8] Y. J. Wang, X. Z. Lin, W. Lan, T. Kohler, M. C. Lux-Steiner, R. Klenk, Phys. Status. Solidi **14**(6), 1600169 (2017).
[9] D. B. Mitzi, M. Yuan, W. Liu, A. J. Kellock, S. J. Chey, V. Deline, A.G. Schrott, Adv. Mater. **20**(19), 3657 (2008).
[10] W. Liu, D. B. Mitzi, M. Yuan, A. J. Kellock, S. J. Chey, O. Gunawan, Chem. Mater. **22**(3), 1010 (2010).
[11] T. K. Todorov, O. Gunawan, T. Gokmen, D. B. Mitzi, Prog. Photovolt: Res. Appl. **21**(1), 82 (2013).
[12] W. H. Hsu, H. I. Hsiang, M. H. Chen, C. C. Chen, S. Zhang, J. Am. Ceram. Soc. **97**(8), 2439 (2014).
[13] R. Krishnan, D. Wood, V. U. Chaudhari, E. A. Payzant, R. Noufi, S. Rozeveld, W. K. Kim, T. J. Anderson, Prog. Photovolt: Res. Appl. **20**(5), 543 (2012).
[14] Y. Zhou, L. Wang, S. Chen, S. Qin, X. Liu, J. Chen, D. J. Xue, M. Luo, Y. Cao, Y. Cheng, E. H. Sargent, J. Tang, Nat. Photonics **9**(6), 409 (2015).
[15] H. Liu, Z. Jin, W. Wang, J. Li, Cryst. Eng. Comm. **13**(24), 7198 (2011).
[16] J. Weszka, P. Daniel, A. Burian, A. M. Burian, A.T. Nguyen, J. Non-Cryst. Solids **265**(1), 98 2000).
[17] S. M. Wasim, C. Rincón, G. Marín, J. M. Delgado, J. Contreras, J. Phys. D Appl. Phys. **37**(3),

479 (2004).
[18] K. G. Deepa, K. P. Vijayakumar, C. Sudhakartha, Mat. Sci. Semicon. Proc. **15**(2), 120 (2012).
[19] W. Witte, R. Kniese, M. Powalla, Thin Solid Films **517**(2), 867 (2008).
[20] B. Minceva-Sukarova, M. Najdoski, I. Grozdanov, C.J. Chunnilall, J. Mol. Struct. **s 410-411**, 267 (1997).
[21] C. Rincón, S. M. Wasim, G. Marín, J. M. Delgado, J. R. Huntzinger, A. Zwick, J. Galibert, Appl. Phys. Lett. **73**(4), 441 (1998).
[22] J. Jiang, S. Yu, Y. Gong, W. Yan, R. Zhang, S. Liu, W. Huang, H. Xin, Sol. RRL **2**(6), 1800044 (2018).
[23] C. H. Ho, Sci. Rep. **4**, 4764 (2014).
[24] J. S. Park, Z. Dong, S. Kim, J. H. Perepezko, J. Appl. Phys. **87**(8), 3683 (2000).
[25] G. Dagan, T. F. Ciszek, D. Cahen, J. Phys. Chem. **96**(26), 11009 (1992).
[26] S. B. Zhang, S. H. Wei, Phys. Rev. B **65**(8), 081402 (2002).
[27] W. Ding, J. Zhu, Z. Wang, Y. Gao, D. Xiao, Y. Gu, Z. Zhang, W. Zhu, Nat. Commun. **8**, 14956 (2017).
[28] T. Zhai, Y. Ma, L. Li, X. Fang, M. Liao, Y. Koide, J. Yao, Y. Bando, D. Golberg, J. Mater. Chem. **20**(32), 6573 (2010).
[29] Y. Min, G.D. Moon, J. Park, M. Park, U. Jeong, Nanotechnology **22**(46), 465604 (2011).
[30] H. Takahashi, H. Fujiki, S. Yokoyama, T. Kai, K. Tohji, Nanomaterials **8**(4), 221 (2018).
[31] C. Rincón, F.J. Ramírez, J. Appl. Phys. **72**(9), 4321 (1992).
[32] X. Fontané, V. Izquierdo-Roca, L. Calvo-Barrio, J. Álvarez-Garcia, A. Pérez-Rodríguez, J. R. Morante, W. Witte, Appl. Phys. Lett. **95**(12), 121907 (2009).
[33] S. Shirakata, H. Kubo, C. Hamaguchi, S. Isomura, Jap. J. Appl. Phys. **36**(10), 1394 (1997).
[34] J. Álvarez-García, B. Barcones, A. Pérez-Rodríguez, A. Romano-Rodríguez, J. R. Morante, A. Janotti, S. H. Wei, R. Scheer, Phys. Rev. B **71**(5), 054303 (2005).
[35] C. J. Hibberd, K. Ernits, M. Kaelin, U. Müller, A. N. Tiwari, Prog. Photovolt: Res. Appl. **16**(7), 585 (2008).
[36] V. M. Glazov, A. S. Pashinkin, V. A. Fedorov, Inorg. Mater. **36**(7), 641 (2000).
[37] S. Kim, W. K. Kim, R. M. Kaczynski, R. D. Acher, S. Yoon, T. J. Anderson, O. D. Crisalle, E. A. Payzant, S. S. Li, J. Vac. Sci. Technol. A **23**(2), 310 (2005).
[38] R. Noufi, R. Axton, C. Herrington, S. K. Deb, Appl. Phys. Lett. **45**(6), 668 (1984).